

$(\text{La}_{2/5}\text{Ba}_{2/5}\text{Ca}_{1/5})(\text{Mn}_{(2/5)-x}\text{Ni}_x\text{Ti}_{3/5})\text{O}_3$: Rietveld studies, dielectric and magnetic properties of new perovskite-related oxides

PIKA JHA, SAROJ L SAMAL, KANDALAM V RAMANUJACHARY[†],
SAMUEL E LOFLAND[‡] and ASHOK K GANGULI*

Department of Chemistry, Indian Institute of Technology, Hauz Khas, New Delhi 110 016, India

[†]Department of Chemistry and Biochemistry, [‡]Department of Physics and Astronomy, Rowan University, 201 Mullica Hill Road, Glassboro, NJ 08028, USA

MS received 21 February 2005; revised 5 May 2005

Abstract. Oxides of the type $(\text{La}_{2/5}\text{Ba}_{2/5}\text{Ca}_{1/5})(\text{Mn}_{(2/5)-x}\text{Ni}_x\text{Ti}_{3/5})\text{O}_3$ ($0 \leq x \leq 0.4$) have been synthesized by the ceramic route. All the above oxides have been found to crystallize in the cubic perovskite structure. Rietveld refinement of the Ni-based oxide, $(\text{La}_{2/5}\text{Ba}_{2/5}\text{Ca}_{1/5})(\text{Ni}_{2/5}\text{Ti}_{3/5})\text{O}_3$ gave rise to a composition $(\text{La}_{0.44}\text{Ba}_{0.38}\text{Ca}_{0.18})(\text{Ni}_{0.42}\text{Ti}_{0.58})\text{O}_{2.85(6)}$ and the refined lattice parameter obtained was 3.9411(2) Å (space group $Pm\bar{3}m$; $R(F^2) = 0.026$, $R_p = 0.074$, $wR_p = 0.087$). A shift from antiferromagnetic to paramagnetic behaviour is observed with increase in nickel concentration, the Mn-rich phases showing antiferromagnetism around 5 K. There is a systematic decrease in the dielectric constant, ϵ and loss tangent with increase in Ni concentration (from $\epsilon = 592$ for $x = 0$ to $\epsilon = 78$ for $x = 0.4$).

Keywords. Oxides; Rietveld studies; dielectric.

1. Introduction

A variety of oxides showing interesting magnetic properties belong to the perovskite structure. The rare-earth-based manganates are perhaps the most widely studied among the perovskite-based magnetic oxides. These oxides can exhibit a range of properties and shot into prominence with the discovery of colossal magnetoresistance (Jin *et al* 1994). Oxides based on LaMnO_3 (Laiko *et al* 2003) are well known for their antiferromagnetic behaviour as well as for their giant magnetoresistance. Substitution of La by monovalent alkali or divalent alkaline earth metal ions induces ferromagnetic behaviour in these oxides. Such substitution of lower valent ions for La^{3+} ions results in mixed valence at the Mn site, allowing the hopping of $\text{Mn}^{+3} e_g$ electrons to the neighbouring Mn^{4+} site. This introduces a long-range ferromagnetic spin ordering through the double exchange mechanism (Zener 1951). For example, oxides like $\text{La}_{0.7}\text{Ca}_{0.3}\text{MnO}_3$ (Huang *et al* 2003), $\text{La}_{1-x}\text{Pb}_x\text{MnO}_3$ (Popov *et al* 2003) and $\text{La}_{1-x}\text{Sr}_x\text{MnO}_3$ (Pinsard *et al* 1997), show electron spin ordering along with magnetoresistance. The perovskite oxides of the type $\text{Ln}_{1-x}\text{A}_x\text{MnO}_3$ (A = Ca, Sr, Pb etc), are specially interesting because they show long range ordering of the Mn^{+3} ($t_{2g}^3 e_g^1$) and Mn^{+4} ($t_{2g}^3 e_g^0$) ions which is linked to the antiferromagnetic spin ordering (Rao 2000).

Though there has been a great deal of work in the area of rare-earth manganates, limited effort has gone into the study of perovskites with transition-metal ions and Ti^{4+} in the B-sites. In one study (Li *et al* 2000) on $\text{Ln}_{2/3}\text{Ca}_{1/3}\text{Mn}_{1-x}\text{Ti}_x\text{O}_3$ ($0 \leq x \leq 0.3$), it was found that substitution of Mn^{4+} by nonmagnetic Ti^{4+} ion significantly suppresses the ferromagnetism and double exchange mechanism, and favours intragrain fluctuation. In another study (Ramanujachary and Swamy 1981), $\text{La}_2\text{MnTiO}_6$ was found to be a *p*-type semiconductor. Long-range antiferromagnetic ordering was reported in ordered double perovskites, La_2TiMO_6 (M = Co and Ni), and the magnetic ordering is attributed solely to Co and Ni ions in the structure (Rodriguez *et al* 2002). Rodriguez *et al* have examined the structure and magnetic properties of $\text{LaNi}_{1-x}\text{Ti}_x\text{O}_3$ system and reported metal–insulator transitions as well as compositionally controlled electron delocalization effects. We have recently reported (Jha *et al* 2004) the synthesis and characterization of a new titano-manganate $(\text{La}_{2/5}\text{Ba}_{2/5}\text{Ca}_{1/5})(\text{Mn}_{2/5}\text{Ti}_{3/5})\text{O}_3$, with a high concentration of titanium (60%) in the B-site of the ABO_3 perovskite structure and obtained a bi-functional oxide with antiferromagnetic behaviour (Neel temperature, $T_N \sim 5$ K) and high dielectric constant (592 at 100 kHz). These interesting properties of this oxide prompted us to investigate solid solutions of similar composition $(\text{La}_{2/5}\text{Ba}_{2/5}\text{Ca}_{1/5})(\text{Mn}_{(2/5)-x}\text{Ni}_x\text{Ti}_{3/5})\text{O}_3$ ($0 \leq x \leq 0.4$). Here, we report the synthesis, structural characterization by Rietveld analysis, compositional analysis, magnetic and dielectric properties of the above family of oxides.

*Author for correspondence (ashok@chemistry.iitd.ernet.in)

2. Experimental

(La_{2/5}Ba_{2/5}Ca_{1/5})(Mn_(2/5-x)Ni_xTi_{3/5})O₃ oxides were prepared by the ceramic method. Stoichiometric amounts of La₂O₃ (CDH, 99.9%), TiO₂ (Fluka, 99.9%), CaCO₃ (Merck, 98.5%), BaCO₃ (Loba Chemie, 99%), NiCO₃ (Qualigens, minimum Ni assay, ~45%) and MnCO₃ (CDH, minimum Mn assay, ~46%) were taken. The rare-earth oxides were dried at 900°C for 6 h before weighing, while the other oxides and carbonates were dried at 150°C. The reactants were thoroughly mixed in an agate mortar and heated in alumina boats at 900°C for 12 h and 1025°C for 48 h followed by heating at 1100°C for 40 h with intermittent grinding. The resulting powder was ground, mixed with 5% PVA (polyvinyl alcohol) solution and compacted into pellets with a force of 4 tons. The pellets were then sintered at 1100°C for 3 h. Powder X-ray diffraction was carried out after each step with a Bruker D 8 Advance diffractometer with Cu-K_α radiation. A step size of 0.05° in 2 theta with step time of 1 s was used for the 2-theta range of 10 to 70 degrees. The raw data was subjected to background correction and K_{α2} stripping. Lattice parameters were refined by a least squares fit of the observed *d*-values. For Rietveld analysis, a step size of 0.02° and a step time of 6 s was used. Refinement was carried out using the GSAS software (Larson and Von Dreele 1994). Standard procedure was followed for the refinement. The final refinement cycle consisted of variables including the cell parameter, scale factor, the zero-point correction, the absorption correction, the profile, six terms of the background fitting polynomial (shifted Chebyshev) and the isotropic thermal parameters. Oxygen-site occupancy was refined as well.

Scanning electron micrographs (SEM) were obtained on sintered disks with a Cambridge Stereoscan 360 electron microscope. Energy dispersive analysis of X-rays (EDX) has been carried out on a LEO 4401 electron microscope by integrating it with an Oxford ISIS EDX system. Magnetic data were collected with a Quantum Design, physical property measuring system (PPMS) in the temperature range 10–300 K. Both a.c. and d.c. magnetization studies were carried out at zero and applied d.c. magnetic field, *H*.

The dielectric constant was measured on disks coated with silver using a HP 4284 L LCR meter in the frequency range 50 Hz–500 kHz. Measurement of the dielectric constant and dielectric loss was carried out between room temperature and 673 K. The density of the sintered disks was estimated by the Archimedes method with CCl₄ as the solvent. The disks were soaked in the organic medium for 36 h and weights were taken till a constant weight was observed. For consistency, three different density measurements were carried out for each sample. The actual density was found to vary between 92 and 94% of theoretical density.

3. Results and discussion

The powder X-ray diffraction studies of the above oxides after heating at 900°C show the formation of two perovskite phases with reflections close to those of LaMO₃ (M = Mn, Ni) and CaTiO₃. After heating at 1025°C for 48 h, a small amount of CaTiO₃ is observed along with the major perovskite phase. A final heating at 1100°C lead to the formation of pure cubic phases corresponding to (La_{2/5}Ba_{2/5}Ca_{1/5})(Mn_(2/5-x)Ni_xTi_{3/5})O₃. It is observed that solid solutions are formed for the entire range of composition (0 ≤ *x* ≤ 0.4) (figure 1). With increase in Ni content the reflections shift towards the higher *d*-values. The diffraction pattern could be indexed based on a cubic cell with the lattice parameter, *a* = 3.9456 (4) Å for (La_{2/5}Ba_{2/5}Ca_{1/5})(Ni_{2/5}Ti_{3/5})O₃. We have not found any indication of the five-layered ordered perovskite structure as has been earlier reported for the cupro-titanates, Ln₂Ba₂CaCu₂Ti₃O₁₄ (Zhu *et al* 1995; Pack *et al* 1997). Note that the composition (La_{2/5}Ba_{2/5}Ca_{1/5})(Mn_{2/5}Ti_{3/5})O₃ chosen by us is equivalent to the formula Ln₂Ba₂CaM₂Ti₃O₁₄, corresponding to the five-layered structure. However, in the absence of any ordering, the disordered cubic perovskite (as obtained in our studies) is better represented as (La_{2/5}Ba_{2/5}Ca_{1/5})(Mn_{2/5}Ti_{3/5})O₃. The lack of cationic order in the present compounds with transition metal ions in the B-site is similar to the results obtained on the related oxide (Ln_{2/5}Ba_{2/5}Ca_{1/5})(Zn_{2/5}Ti_{3/5})O₃ (Jha and Ganguli 2003; Jha *et al* 2003). Annealing in air or oxygen for 5 days followed by slow cooling did not lead to any ordering of the cations (tetragonal structure).

In these oxides, manganese is expected to be present in the trivalent state, while nickel is expected in the divalent state. The ionic radius of Ni²⁺ (0.690 Å) is higher than that of Mn³⁺ (0.645 Å). This increase in ionic radius accounts for the higher lattice parameters with increase in Ni. The refined lattice parameters as obtained by a least-squares fit to the observed *d* values are given in table 1. Note that the pure Mn compound (*x* = 0) has a lattice parameter *a* = 3.9261(4) (Jha *et al* 2004).

Rietveld refinement of powder X-ray data was carried out on (La_{2/5}Ba_{2/5}Ca_{1/5})(Ni_{2/5}Ti_{3/5})O₃. The La, Ba and Ca ions were statistically allocated to the 1a site with 100% occupancy, and the transition metal ions were statistically allocated to the 1b site with 100% occupancy. The structure refined to reasonable *R*-values (*R*(*F*²) = 0.026, *R*_p = 0.074, *wR*_p = 0.087) in the space group *Pm* $\bar{3}$ *m*. In case of the oxide, (La_{2/5}Ba_{2/5}Ca_{1/5})(Ni_{2/5}Ti_{3/5})O₃, the region in the 2-theta range of 28.74°–29.1° was excluded, since in this region a reflection corresponding to a minor impurity phase was present. This impurity could not be characterized satisfactorily. We have carried out TEM analysis on the Mn-based oxide, and only the reciprocal lattice corresponding to the simple cubic structure was seen with no evidence of superlattice formation (Jha *et al* 2004). The

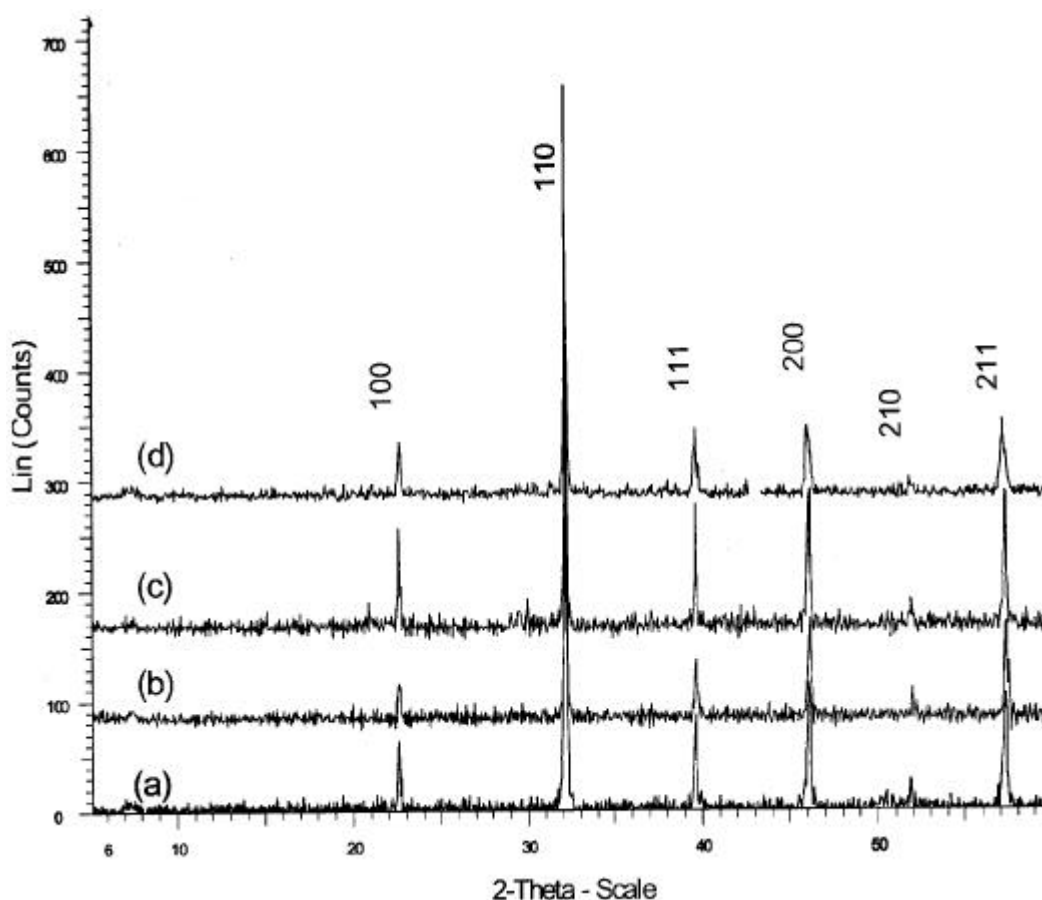


Figure 1. Powder X-ray diffraction pattern for $\text{La}_{2.5}\text{Ba}_{2.5}\text{Ca}_{1.5}\text{Mn}_{(2.5-x)}\text{Ni}_x\text{Ti}_{3.5}\text{O}_3$ for $x =$ (a) 0.1, (b) 0.2, (c) 0.3 and (d) 0.4.

Table 1. Refined lattice parameters for $\text{La}_{2.5}\text{Ba}_{2.5}\text{Ca}_{1.5}\text{Mn}_{(2.5-x)}\text{Ni}_x\text{Ti}_{3.5}\text{O}_3$ with different values of 'x' (the e.s.d.'s are given in parentheses).

Composition (x)	Lattice parameter, a (Å)
0.1	3.9277(5)
0.2	3.9301(5)
0.3	3.9423(6)
0.4	3.9456(3)

final refined composition obtained was $(\text{La}_{0.44}\text{Ba}_{0.38}\text{Ca}_{0.18})(\text{Ni}_{0.42}\text{Ti}_{0.58})\text{O}_{2.85(6)}$ and the refined lattice parameter obtained was 3.9411(2) Å. The final refined values of isotropic thermal factors, occupancies and Wyckoff symbols for this composition are listed in table 2. The observed, calculated and the difference plot are shown in figure 2. Rietveld studies on the oxide $(\text{La}_{2.5}\text{Ba}_{2.5}\text{Ca}_{1.5})(\text{Mn}_{2.5}\text{Ti}_{3.5})\text{O}_3$ also showed that it was cubic with a lattice parameter of 3.9477(23) Å (Jha *et al* 2004).

Scanning electron micrograph for $(\text{La}_{2.5}\text{Ba}_{2.5}\text{Ca}_{1.5})(\text{Mn}_{(2.5-x)}\text{Ni}_x\text{Ti}_{3.5})\text{O}_3$ has been obtained on the disks compacted under 8 tons of force and sintered at 1100°C. The

grains have an average grain size of 0.5 μm for the oxide with $x = 0$ and the grains are spherical in shape (Jha *et al* 2004). The SEM micrographs of the oxide with $x = 0.2$ show partially melted grains with average size in the range of 0.5–0.7 μm (figure 3(a)). However, the oxide with $x = 0.4$ has very well defined spherical grains which are slightly larger in size (1.0 μm) as shown in figure 3(b).

For the oxide $(\text{La}_{2.5}\text{Ba}_{2.5}\text{Ca}_{1.5})(\text{Mn}_{1.5}\text{Ni}_{1.5}\text{Ti}_{3.5})\text{O}_3$, the composition obtained from EDX studies was found to be $(\text{La}_{0.44(1)}\text{Ba}_{0.42(1)}\text{Ca}_{0.18(1)})(\text{Mn}_{0.15(1)}\text{Ni}_{0.17(1)}\text{Ti}_{0.56(1)})\text{O}_{2.70}$. On renormalization of the composition with respect to A-site occupancy, a composition of $(\text{La}_{0.42}\text{Ba}_{0.40}\text{Ca}_{0.17})(\text{Mn}_{0.14}\text{Ni}_{0.16}\text{Ti}_{0.54})\text{O}_{2.62}$ was obtained. In case of the oxide with loaded composition $(\text{La}_{2.5}\text{Ba}_{2.5}\text{Ca}_{1.5})(\text{Mn}_{2.5}\text{Ti}_{3.5})\text{O}_3$, the EDX results led to the composition of $(\text{La}_{0.44(1)}\text{Ba}_{0.40(1)}\text{Ca}_{0.18(1)})(\text{Mn}_{0.33(1)}\text{Ti}_{0.57(1)})\text{O}_{2.71}$ (Jha *et al* 2004). Thus the calculated composition was quite close to the loaded composition in all the cases.

Iodometric titration was carried out to calculate the average oxidation states of the transition metal ion. For the Ni-based oxide, no iodine was liberated and hence it was concluded that all Ni is in the divalent state. How-

ever, around 4% of Mn was found to be in the tetravalent state, and the average Mn oxidation state was 3.04 (Jha et al 2004).

The oxide with nominal composition $(\text{La}_{2/5}\text{Ba}_{2/5}\text{Ca}_{1/5})(\text{Mn}_{2/5}\text{Ti}_{3/5})\text{O}_3$ was found to be antiferromagnetic at 5 K, although the details are difficult to determine due to minor (~1%) impurity phases of alkaline-earth doped rare-earth manganates which could not be seen by X-ray studies (Jha et al 2004). As seen in figure 4, for $x = 0.1$, the a.c. susceptibility in the paramagnetic state is rather unusual at zero field due to these impurities. However, applying a d.c. field of 5 kOe, which magnetically saturates the ferromagnetic impurities and has no effect on the paramagnetic component of the bulk of the sample (inset figure 4), the results are more reasonable. In the case of $x = 0.1$ though, even at 5 kOe, there is contribution from the impurities.

Figure 5 shows the Curie plots for several compositions with the fits. Assuming that average Mn valence is

3.04 [(0.96 Mn^{3+} ($3d^4$) and 4% Mn^{4+} ($3d^3$)] and that of Ni is 2 (Ni^{2+} $3d^8$), the effective moment per mole-formula unit is

$$m = \sqrt{(0.4 - x)[0.96 * (4 * 6) + 0.04 * (3 * 5)] + x(2 * 4)}. \quad (1)$$

Figure 6 gives the expected (1) and experimentally determined m values as function of x , and the inset displays the compositional dependence of the Weiss temperature, Θ . The m values agree reasonably well, particularly considering the small variation in the final composition as compared to the loaded one. Note that Θ is positive for $x = 0$ and becomes negative with increasing $x = 0.4$, suggesting the presence of ferromagnetic interactions for small x , even though earlier studies seemed to indicate that $x = 0$ is antiferromagnetic. It is very likely that there is a competition between antiferromagnetic superexchange and ferromagnetic Zener double exchange which takes place in samples with small x values which possess non-

Table 2. Positional, thermal and occupancy factors of $(\text{La}_{0.44}\text{Ba}_{0.38}\text{Ca}_{0.18})(\text{Ni}_{0.42}\text{Ti}_{0.58})\text{O}_{2.85(6)}$ after refinement of powder X-ray data.

Atoms	Wyckoff symbol	Occupancy	x	y	z	Uiso*100
La	1a	0.44	0.0	0.0	0.0	0.33(8)
Ba	1a	0.38	0.0	0.0	0.0	0.33(8)
Ca	1a	0.18	0.0	0.0	0.0	0.33(8)
Ni	1b	0.42	0.5	0.5	0.5	1.48(2)
Ti	1b	0.58	0.5	0.5	0.5	1.48(2)
O	3c	0.95(2)	0.0	0.5	0.5	2.60(12)

Space group $Pm\bar{3}m$; 'a' = 3.9411(2), $R(F^2) = 0.026$, $R_p = 0.074$, $wR_p = 0.087$.

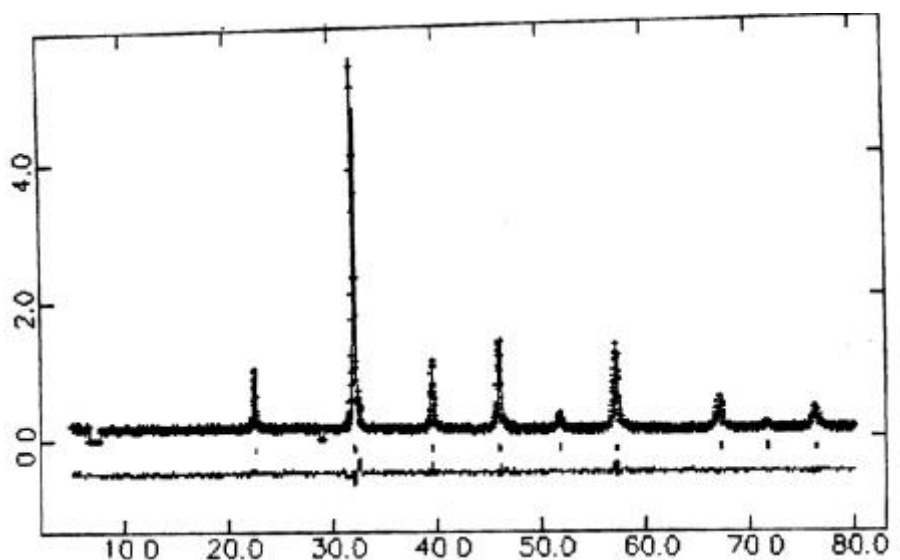


Figure 2. Observed, calculated and difference pattern of the oxide with refined composition $(\text{La}_{0.44}\text{Ba}_{0.38}\text{Ca}_{0.18})(\text{Ni}_{0.42}\text{Ti}_{0.58})\text{O}_{2.85(6)}$ as obtained by Rietveld refinement of powder X-ray data.

zero electrical conductivity (see below). This competition probably also accounts for the difference between the large Θ value (47 K) for $x = 0$ yet its low T_N (~ 5 K).

The dielectric properties of the above oxides have been studied in detail with respect to frequency and temperature. The dielectric constant, ϵ , and loss tangent, $\tan d$, at 308 K at a frequency of 100 kHz are shown as functions of x in figure 7. It is seen that with increasing x , both ϵ and $\tan d$ decrease. The $x = 0$ material has been reported to have a high dielectric constant of 590 (Jha *et al* 2004). Figure 8a shows the frequency dependence of ϵ and $\tan d$ for $x = 0.2$ at 308 K while figure 8b shows the temperature dependence of ϵ and $\tan d$ of the same compound at 100 kHz. Both ϵ and $\tan d$ are highly dependent on frequency and temperature with ϵ steadily decreasing with frequency. One reason for this behaviour may be that the grain boundaries are effective at lower frequencies (Koops 1951). On the other hand, $\tan d$ shows a peak around 50 kHz. With temperature, ϵ increases slowly up to

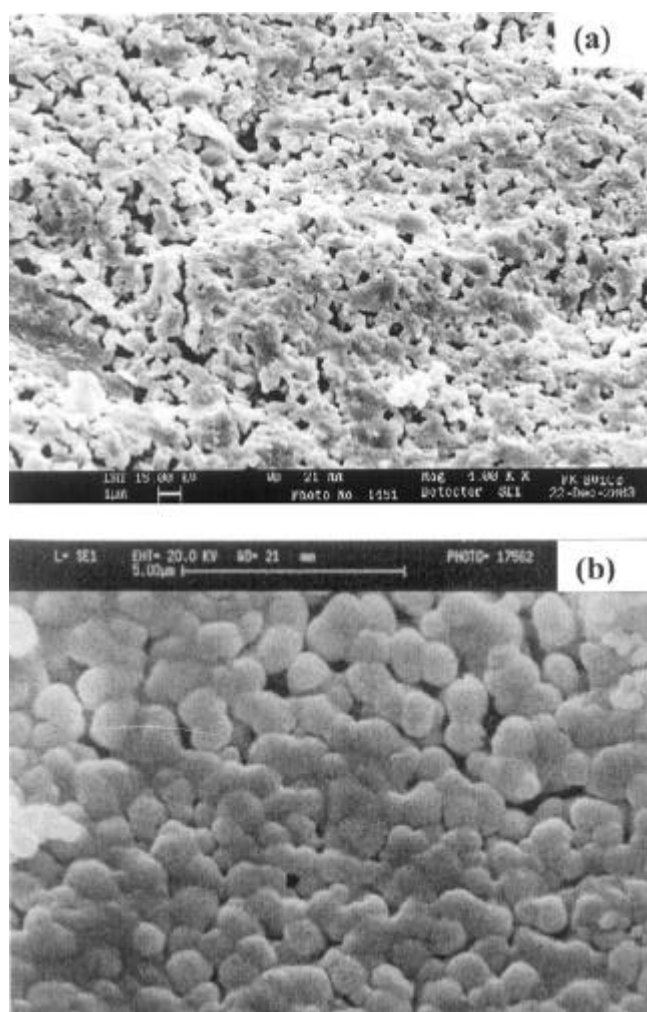


Figure 3. Scanning electron micrographs of oxides with loaded composition $(\text{La}_{2/5}\text{Ba}_{2/5}\text{Ca}_{1/5})(\text{Mn}_{(2/5-x)}\text{Ni}_x\text{Ti}_{3/5})\text{O}_3$ for $x =$ (a) 0.2 and (b) 0.4.

373 K, beyond which it shows a steep rise up to 473 K while $\tan d$ increases from 1.47 at room temperature to 2.35 at 473 K. This is probably because of the fact that the electron hopping between adjacent Mn^{3+} and Mn^{4+} is

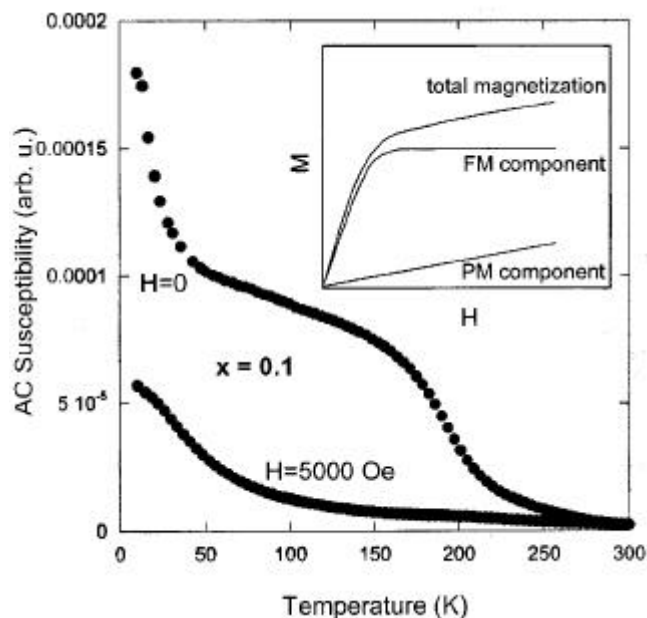


Figure 4. Temperature dependence of $(\text{La}_{2/5}\text{Ba}_{2/5}\text{Ca}_{1/5})(\text{Mn}_{2/5}\text{Ti}_{3/5})\text{O}_3$ of the a.c. susceptibility of $x = 0.1$ at $H = 0$ and 5 kOe. The presence of minor ferromagnetic impurity phases dominate the susceptibility at low field. The inset shows a schematic of the effect of magnetic field on the magnetization and demonstrates that for H larger than the magnetic saturation field of the impurity, the measured a.c. susceptibility should be close to the intrinsic susceptibility of the bulk sample.

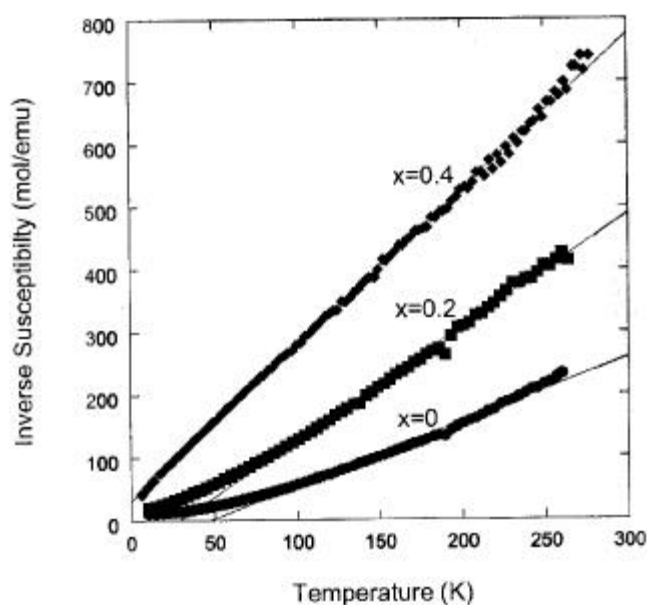


Figure 5. Curie plots of several samples of $(\text{La}_{2/5}\text{Ba}_{2/5}\text{Ca}_{1/5})(\text{Mn}_{(2/5-x)}\text{Ni}_x\text{Ti}_{3/5})\text{O}_3$. The lines represent linear fits of the data between 100 and 270 K.

thermally activated, which leads to higher ϵ values at elevated temperatures. Related studies on the electron hopping mechanism and dielectric properties have been reported for α -Fe₂O₃ (Papaioannou *et al* 2005) and in rare earth manganates (Sudheendra and Rao 2003). Concomitantly, the large value of $\tan d$ implies some electronic conduction which also occurs primarily by hopping. Therefore, ϵ and $\tan d$ both increase as the temperature increases.

For (La_{2/5}Ba_{2/5}Ca_{1/5})(Ni_{2/5}Ti_{3/5})O₃, ϵ and $\tan d$ are 78 and 0.21, respectively, at room temperature and 100 kHz (figure 9(a)). As expected, ϵ shows a decrease with frequency ($\epsilon = 59$ at 500 kHz). The temperature dependence, however, is markedly different from that of $x = 0$ (figure 9b) where there is an increase of ϵ (figure 9(b))

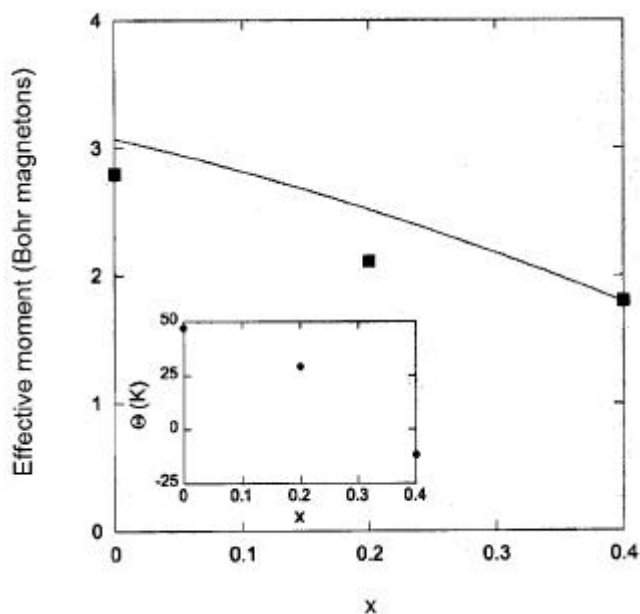


Figure 6. Dependence of effective magnetic moment on x . The line represents the expected values determined via (1). The inset shows the variation of the Weiss temperature with x .

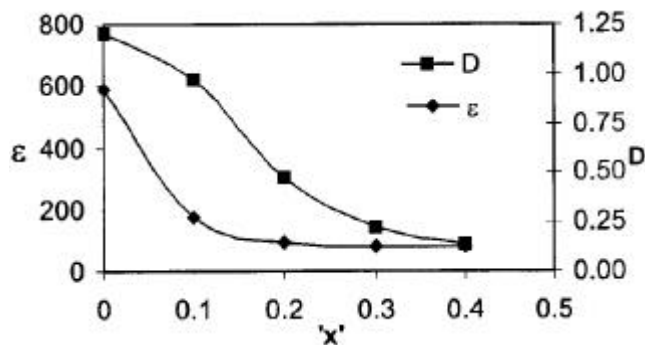


Figure 7. Plot of variation of dielectric constant and dielectric loss with x for (La_{2/5}Ba_{2/5}Ca_{1/5})(Mn_(2/5-x)Ni_xTi_{3/5})O₃ at 100 kHz. The data for $x = 0$ composition is taken from an earlier study (Jha *et al* 2004).

and decrease in $\tan d$ beyond 423 K. Overall, the dependence of the dielectric properties with respect to frequency and temperature are much less pronounced for the

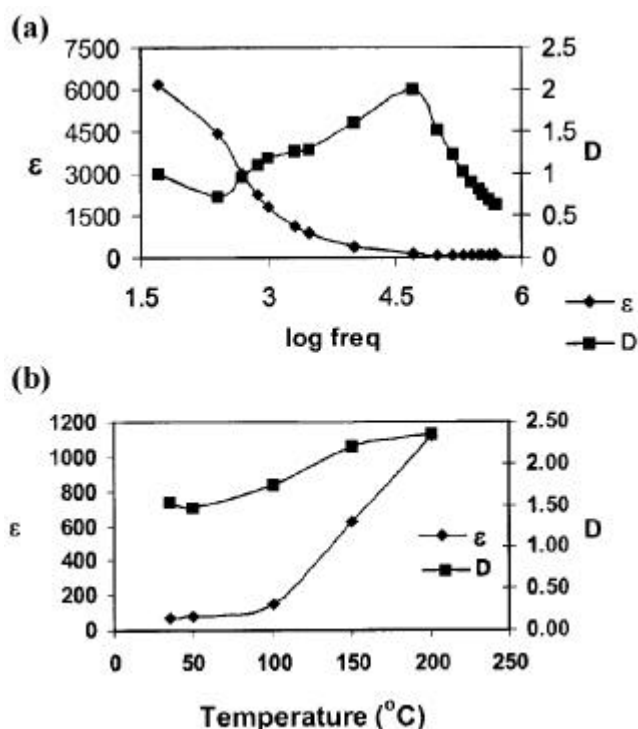


Figure 8. Plot of variation of dielectric constant and dielectric loss for (La_{2/5}Ba_{2/5}Ca_{1/5})(Mn_(2/5-x)Ni_xTi_{3/5})O₃ for $x = 0.2$ with (a) frequency and (b) temperature at 100 kHz.

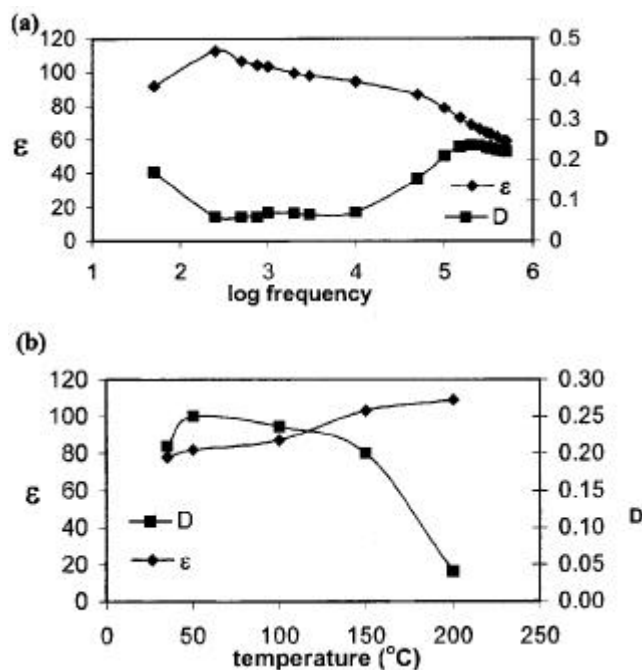


Figure 9. Plot of variation of dielectric constant and dielectric loss for (La_{2/5}Ba_{2/5}Ca_{1/5})(Ni_{2/5}Ti_{3/5})O₃ with (a) frequency and (b) temperature at 100 kHz.

Ni-based oxide as compared to those of the pure Mn-based oxide (Jha *et al* 2004). Since iodometric estimations have shown that Ni is present only in the divalent state, the possibility of electron hopping between adjacent sites is absent, which makes the dielectric properties less sensitive to variation in frequency and temperature.

4. Conclusions

We have synthesized novel titanates of the formula $(\text{La}_{2/5}\text{Ba}_{2/5}\text{Ca}_{1/5})(\text{Mn}_{(2/5-x)}\text{Ni}_x\text{Ti}_{3/5})\text{O}_3$. Solid solutions have been obtained for the entire range of compositions studied. These oxides crystallize in the cubic perovskite structure. The Mn-rich phases show weak antiferromagnetic behaviour below 10 K. However, the pure Ni-based oxide is paramagnetic. The above oxides show reasonably high dielectric constants which decrease with increasing Ni, which appears to be related to electronic conduction. Similar behaviour is observed for $\tan d$ as well. Thus Ni substitution in the manganese sites of these rare-earth-based titanates, produce a considerable modulation in the magnetic as well as the dielectric properties.

Acknowledgements

Financial assistance from CSIR, Govt. of India, is gratefully acknowledged. One of the authors (SEL) would like to acknowledge partial support from the NSF MRSEC Grant no. DMR 00-08008.

References

Huang Y-H, Huang K-F, Luo F, He L-L, Wang Z-M, Liao C-S and Yan C-H 2003 *J. Solid State Chem.* **174** 257

- Jha P and Ganguli A K 2003 *Proc. Indian Acad. Sci (Chem. Sci.)* **115** 431
- Jha P, Bobev S, Subbanna G N and Ganguli A K 2003 *Chem. Mater.* **15** 2229
- Jha P, Sarita R, Ramanujachary K V, Lofland S E and Ganguli A K 2004 *J. Solid State Chem.* **177** 2881
- Jin S, Tiefel T H, McCormack N, Fastnacht R A, Ramesh R and Chen J-H 1994 *Science* **264** 413
- Koops C G 1951 *Phys. Rev.* **83** 121
- Laiko R, Lisomov K G, Lahderanta E, Petrenko P A, Salminen J, Stamo V N, Stepsnov Y P and Zakhvalinskii V S 2003 *J. Phys. Chem. Solids* **64** 2313
- Larson A C and Von Dreele R B 1994 *GSAS—General structure analysis system* (Los Alamos, NM: Los Alamos National Laboratory)
- Li R-W, Wong Z-H, Chen X, Sun J, Shen B and Hun C H 2000 *J. Appl. Phys.* **87** 5597
- Pack M J, Gormezano A and Weller M T 1997 *Chem. Mater.* **9** 1547
- Papaioannou J C, Patermarakis G S and Karayianni H S 2005 *J. Phys. Chem. Solids* **66** 839
- Pinsard L, Rodriguez-Carvajal J and Revcolevschi A 1997 *J. Alloys Compds.* **262–263** 152
- Popov G, Goldsmith J and Greenblatt M J 2003 *Solid State Chem.* **175** 52
- Ramanujachary K V and Swamy C S 1981 *Indian J. Chem.* **A20** 96
- Rao C N R 2000 *J. Phys. Chem.* **B104** 5877
- Rodriguez E, Alvarez I, Lopez M L, Veiga M L and Pico C 1999 *J. Solid State Chem.* **148** 479
- Rodriguez E, Lopez M L, Campo J, Veiga M L and Pico C 2002 *J. Mater. Chem.* **12** 2798
- Sudheendra L and Rao C N R 2003 *J. Phys. Cond. Matter* **15** 3029
- Zener C 1951 *Phys. Rev.* **82** 403
- Zhu W J, Huang Y Z, Ning T S and Zhao Z X 1995 *Mater. Res. Bull.* **30** 243